Optics and Lasers in Engineering 141 (2021) 106573

Contents lists available at ScienceDirect

Optics and Lasers in Engineering

journal homepage: www.elsevier.com/locate/optlaseng

Review

Motion induced error reduction methods for phase shifting profilometry: A review

Lei Lu[a,1], Vignesh Suresh[b,1], Yi Zheng[b], Yajun Wang[c], Jiangtao Xi[d], Beiwen Li[b,*]

[a] College of Information Science and Engineering, Henan University of Technology, Zhengzhou, 450001, China
[b] Department of Mechanical Engineering, Iowa State University, Ames, Iowa 50011, USA
[c] Department of Opto-Electronics, Sichuan University, Chengdu 610065, China
[d] School of Electrical Computer and Telecommunications Engineering, University of Wollongong, Wollongong, NSW, 2522, Australia

ARTICLE INFO

Keywords:
3D Shape measurement
High-speed
Structured light
Motion-induced error
Fringe projection
Phase shifting profilometry

ABSTRACT

3D shape measurement using phase shifting profilometry (PSP) has been extensively studied by the researchers in the past few years. With the recent binary defocused method, the measurement speed of these systems have been increased significantly. Yet, measurement errors are inevitable while imaging dynamic scenes. This is mainly because PSP methods require the object to be static for a short period of time. Researchers have developed various methods to alleviate the motion-induced errors for PSP systems. This paper reviews the various state-of-the-art motion-induced error reduction methods. The various research methods are categorized into different groups and the principles behind each method was explained. We conducted experiments to compare the potential of different algorithms in compensating the motion-induced errors. A comparative discussion is also provided to serve as a reference for selection of methods under different application scenarios. Finally, further discussions are also provided to point out opportunities for future research in this field.

1. Introduction

All objects that exist in the world are three dimensional (3D), and thus the acquisition of 3D geometric data can provide more information compared to the two dimensional (2D) images. 3D geometric data acquisition technologies have attracted intensive attentions by the researchers and lots of algorithms are developed to reconstruct the objects for different applications. The 3D shape measurement technology [1] is widely used in many fields such as automobile, manufacturing and entertainment industries.

The 3D shape measurement methods can be broadly classified into two categories: (i) contact methods and (ii) non-contact methods. Coordinate measuring machine (CMM) [2,3] is the most typical measurement system employing the contact method. CMM acquires the 3D coordinate information by using a probe to detect the object surface (by touching) [4,5]. Though CMMs have an accuracy in sub-micrometer level, their point-by-point nature with a touching probe limits the speed of measurements, not to mention the risk of causing damage to the objects surface (especially soft objects) during measurements [6]. Over the past decades, researchers have developed many non-contact 3D shape measurement methods. Some of them include laser triangulation scanner [7], time of flight scanner [8,9], depth from defocus [10,11], stereo vision [12,13] and structured light [14]. Structured light is one of the most popular techniques as it can perform simultaneous high-speed and high-accuracy 3D shape measurement [15].

A typical structured light system includes one camera and one projector. The projector projects structured light pattern onto the object surface and the camera captures the reflected pattern from another angle. Because of the geometry of the object, the captured structured light pattern will be distorted. The 3D geometry of the object can be retrieved by analyzing the difference between the distorted pattern and the projected pattern. Among all the existing structured light methods, the method based on sinusoidal fringe pattern employing the phase information has been proven capable of achieving robust measurement given that phase information is robust to noise, ambient light or reflectivity variations [16]. Among the phase-based approaches, Fourier transform profilometry (FTP) [17] and phase shifting profilometry (PSP) [18] are the most commonly used technologies to retrieve the phase information. FTP can reconstruct the object by only one sinusoidal fringe pattern. By using Fourier transform and filtering, the desired phase component is separated from the background component and the phase value is obtained through the inverse Fourier transform. The FTP approach is suitable for dynamic object reconstruction because it only uses one fringe pattern. However, given that it is typically difficult for the filter to separate the components cleanly and clearly, the robustness of FTP

* Corresponding author.
E-mail address: beiwen@iastate.edu (B. Li).
[1] These authors contributed equally to this work.

https://doi.org/10.1016/j.optlaseng.2021.106573
Received 20 September 2020; Received in revised form 3 February 2021; Accepted 8 February 2021
0143-8166/

is still limited. In contrast, the PSP method which employs multiple sinusoidal fringe patterns can address such limitation [18,19]. In fact, at least three sinusoidal fringe patterns with applied phase shifts are projected onto the object surface. During the calculation of the phase value, the background light and reflectivity is removed, leading to robust phase retrieval and thus accurate 3D shape measurement [20–22].

The phase shifting methods can achieve high accuracy for the static object reconstruction [23]. However, as multiple fringe patterns are required, one of the fundamental assumptions associated with the PSP systems is that the object should remain static or quasi-static during one cycle of pattern projection. This does not hold true in the case of dynamic object reconstruction. While imaging dynamic scenes, the object tends to move within the fringe projection period. Two issues will be caused while imaging a moving object: (1) the position of the object among different fringe patterns will be mismatched; (2) for the same point on the object surface, the ideal phase shift between the fringe patterns will be violated. A motion induced error will be introduced if the traditional phase shifting methods are implemented. The motion-induced error can be alleviated by increasing the projecting and capturing speed of the hardware through bit-wise binary technologies [24,25]. The object can be seen as static when the measurement speed is significantly higher than the moving speed. However, this will lead to increase in hardware cost.

A number of methods have been developed to address the problem of motion-induced errors in PSP systems. One of the approach is to track the position of the object [26–34] in the fringe projection period. The errors caused by the motion in the phase map can be corrected by identifying the trajectory of the object. Manual methods by placing markers [26] and automated object tracking methods by scale-invariant feature transform (SIFT) [28] were proposed to track the motion of the objects. However, most of these methods were limited to tracking the two dimensional (2D) motion of the object.

Another approach to reduce the motion-induced errors is by combining Fourier-based methods [35–39] with PSP methods. 3D shape measurement by FTP [40] is conducted by projecting a single fringe pattern. However, the limitation is that it is sensitive to noise and surface texture variation. On the other hand, 3D shapes measured by PSP methods are robust to noise as the method utilizes multiple phase shifted fringe patterns in phase computation. However, PSP methods require a minimum of three fringe patterns to perform one 3D shape measurement. By combining FTP and PSP, the errors induced by object's motion can be alleviated by FTP and it can be used to update the phase map obtained from PSP methods where high-speed motion is present. However, the quality of such phase map is affected by the inherent limitations of FTP.

Researchers also developed motion error reduction methods by predicting the motion of the object [41–45] in the fringe projection period. These methods compensated the motion-induced error in the phase map by predicting and estimating the motion of the object in the cycle of capturing. The advantage of these methods is that it suitable for high-speed applications and dynamically deformable objects (as it does a pixel-wise error compensation). In addition to the aforementioned methods, there are also other motion error reduction methods [46–48] that compensate the motion errors using Hilbert transform [47] and deep learning [48].

This paper reviews various motion-induced error reduction methods that are applicable to PSP systems. There are a few existing review papers focusing on 3D shape measurements in general [49], phase shifting algorithms [50], high-speed measurement [51] and phase unwrapping methods [52,53]. These papers primarily summarized the advances in topics related to 3D surface topographical measurements and the fringe projection technique, yet an area missing in these technical reviews is that what researchers have done when their measured object violates the stationary or quasi-stationary assumption of object in one cycle of projected pattern sequence. Given that there has been an increasing demand for 3D reconstruction of dynamic objects with high accuracy, it is necessary to provide a review of existing approaches that addresses the motion-induced errors in dynamic 3D shape measurements such that guidance are provided for researchers in selection of different types of methods. Therefore, this paper reviews the existing motion-induced error reduction algorithms and analyzes their advantages, limitations and application scenarios. In this review, we broadly classified the existing approaches into four categories: (i) object tracking, (ii) Fourier assisted methods, (iii) motion prediction and (iv) other methods. The principle behind each individual method will be explained.

The paper is organized as follows: Section 2 will introduce the principles of three-step phase shifting algorithm, motion-induced error and the various motion induced error reduction algorithms, Section 3 describes the comparative experiments that we did to evaluate the performance of the various motion induced error reduction algorithms. Section 4 will discuss the boundaries of existing technologies. Section 4.2 points out some opportunities for future research, and Section 5 summarizes the paper.

2. Principles

This section will introduce the principles of three-step phase shifting algorithm and the motion-induced errors. Then, we will discuss the different methods that the researchers have proposed to address the problem of motion induced errors.

2.1. Phase shifting profilometry

Over the past decades, many algorithms based on phase shifting profilometry have been developed. Among them, the three-step phase shifting profilometry is the preferred one for dynamic measurements as it requires the minimum number of fringe patterns for calculating the phase. A three-step phase shifting profilometry with equal phase shifts can be mathematically described as,

$$I_1(x, y) = I'(x, y) + I''(x, y)\cos[\phi(x, y) - 2\pi/3], \tag{1}$$

$$I_2(x, y) = I'(x, y) + I''(x, y)\cos[\phi(x, y)], \tag{2}$$

$$I_3(x, y) = I'(x, y) + I''(x, y)\cos[\phi(x, y) + 2\pi/3], \tag{3}$$

where $I'(x, y)$ is the average intensity, $I''(x, y)$ represents the intensity modulation, and $\phi(x, y)$ is the phase to be solved for. Simultaneously solving the above three equations will lead to,

$$\phi(x, y) = \tan^{-1}\left[\frac{\sqrt{3}(I_1 - I_3)}{2I_2 - I_1 - I_3}\right], \tag{4}$$

An arctangent function is used so that the phase value obtained from Eq. (4) will range from $-\pi$ to π with a 2π modulus. Spatial or temporal phase unwrapping algorithms could be used to unwrap the phase so that we can get a continuous phase map. The unwrapping process essentially estimates the 2π discontinuous locations and removes the 2π jumps by adding or subtracting $k(x, y)$ multiples of 2π.

$$\Phi(x, y) = \phi(x, y) + k(x, y) \times 2\pi. \tag{5}$$

The 3D geometry can be obtained from the unwrapped phase map. However, the 3D shape estimated using this phase (Eq. (5)) will be an accurate representation of the object's geometry only when the object is static.

2.2. Motion induced error in phase shifting profilometry

The motion-induced error in PSP is illustrated in Fig. 1. Every point in the camera's imaging plane (C_1) corresponds to a point on the object's surface (O_1). This relationship holds true when the object remains static, but if the object moves to a different location in the 3D space, then the same camera point (C_1) will correspond to a different point on the object's surface (O_1'). These two points (O_1, O_1') will correspond to different lines on the projector's imaging plane (P_1, P_1'). This will result in

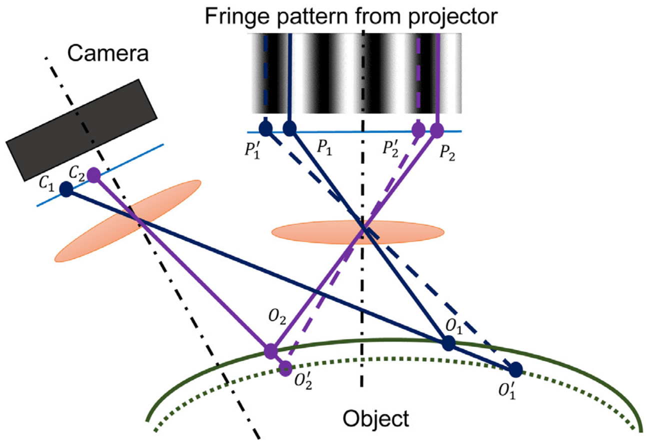

Fig. 1. Schematic of motion induced error in phase shifting profilometry.

two different phase values, Φ_1 and Φ'_1. The difference between the two phases is termed as motion-induced error. In PSP method, the phase is calculated for every pixel, so this error term differs for each pixel (as the motion is not uniform for all the points on the object). Therefore, the 3D coordinate points estimated using this phase map will not be an accurate representation of the object's topography.

2.3. Motion induced error reduction methods

Researchers have proposed many successful methods in the past to address the above mentioned challenge. We have classified those methods into the following four categories.

2.3.1. Object tracking

One of the straight forward approaches to solve the problem of motion-induced error is to track the position of the object within the fringe projection period. Lu et al. [26] tracked the position of the object by placing markers around it. The markers are white colored circles and the center of the circles was chosen as the corresponding points. The circle center was identified from the fringe images and the displacement of the center point (across the fringe images) was represented by the rotation matrix R and translation vector T (estimated by Singular Value Decomposition method). The displacement of the markers represented the displacement of the object. As the system was calibrated by reference plane method, the new height distribution map was calculated using the R and T vector and the corresponding phase (ϕ') was calculated using the relationship between phase and height distribution. This phase shift is incorporated in the fringe pattern images (as shown in Eq. 6) and the wrapped phase was obtained by solving the new set of fringe pattern images. The motion-induced error is significantly reduced by precisely tracking the object's motion during the fringe projection period. However, the method cannot be automated as it requires manual intervention for placing markers that act as cues to estimate the position of the object. They extended the method to compensate for errors introduced by the 3D motion of the object [27]. The 3D motion was restricted to translation in the depth direction. The markers were used to track the 2D motion whereas the phase change due to the motion in depth direction was computed using the iterative algorithm developed by Wang et al. [54]. However, the method does not work when the object undergoes rotation motion.

$$\overline{I}(x, y) = I'(x, y) + I''(x, y)\cos[\phi(x, y) + \phi'(x, y) - 2\pi/3] \tag{6}$$

The same research group [28] automated the method in [26] by tracking the object's position using scale-invariant feature transform (SIFT) algorithm instead of markers. SIFT algorithm is used for detecting features in an image. Along with the phase shifted patterns, features for SIFT is also projected on to the object. The method used different color channels in a color camera to differentiate the fringe patterns from the SIFT features. The fringe patterns were projected in one of the three color channels and this channel was filtered out before performing SIFT. By performing SIFT, the rotation matrix R and translation vector T involved in the motion of the object was estimated and the corresponding phase map ($\phi'(x, y)$) was computed. The 3D image was reconstructed from the new set of phase shifted fringe patterns (as shown in Eq. (6)) using a least-square method. The main advantage of the method is that the entire process is automated and does not require any human intervention as it makes use of the features in the object to reduce the motion-induced errors. But the limitation is that it cannot compensate errors caused by 3D motion as SIFT algorithm will not be able to estimate the change in position of the object in the depth direction. Moreover, both the methods ([26,28]) have limited range of applications as they use reference plane based calibration. This is mainly because the reference plane methods do not have a high accuracy for large scale measurements [55].

Lu et al. [29] proposed another motion-induced error reduction method to address the above mentioned limitations. The object's motion was classified into five different types (three translational and two rotational motion). The authors used a virtual plane to compensate for the motion-induced errors. A general model of the fringe image intensity with the parameters compensating for different kinds of motion was established using the virtual plane. For example, if the object's motion is translational in the $X - Y$ plane, then the compensating parameter will be a function of the shift in position that occurred between the two frames. With this generic model, the motion error was compensated for two types of motion: (i) in-plane translation and (ii) rotation about the axis perpendicular to the virtual plane. The authors used the same approach as proposed in [27] to estimate the in-plane translation whereas the phase change due to rotation was estimated using the advanced iterative least-square algorithm [54] (AIA). The main advantage of this method is that it does not require a reference plane therefore it can be used for a wide range of applications. However, the method works well only for rigid translation and rotation about a perpendicular axis (perpendicular to the virtual plane) and it will be difficult to predict the phase change (for all the pixels) in case of complicated motion like rotation about an oblique axis. Another motion-induced error reduction method using (AIA) [54] was proposed by Flores et al. [30]. The method involved projecting a color fringe pattern on to the object. The fringe patterns required for estimating the phase was encoded in the red (R) channel and a homogeneous white pattern for tracking the object motion was encoded in the blue (BB channel. The phase shift (caused by object motion) is estimated from the white image in B channel by using AIA method [54]. This phase error is then used to rectify the phase map obtained from the fringe patterns. The method does not compromise on the measurement speed as the fringe patterns and homogeneous pattern are projected simultaneously. Therefore, the method is applicable for high-speed applications. However, the measurement speed of this method is limited by the maximum refreshing rate of the projector for colored patterns.

Recently, Lu et al. [31] reconstructed multiple isolated moving objects based on two-frequency phase unwrapping method. In temporal phase unwrapping method (such as two-frequency phase unwrapping method), we can unwrap the multiple isolated objects correctly by projecting additional fringe patterns. The object's movement during the phase shifting fringe pattern and additional fringe pattern will introduce errors to the fringe order determination. By analyzing the influence caused by the shift on the phase map before movement and after movement, the correct relationship between the phase shifting fringe pattern and additional fringe pattern can be obtained. Finally, the correct fringe order is determined by the two-frequency phase unwrapping method.

The method in [31] only can reconstruct multiple objects with the same movement. In dynamic scenes, it is common that multiple objects with different movements are present. Lu et al. [34] proposed an automated method to track and reconstruct multiple objects with individual movement. The objects are identified automatically and the corresponding bounding boxes defining the area occupied by each object are given. Then, the Kernelized Correlation Filters (KCF) is applied to track the object movement in the successive fringe pattern. The movement for each object are described mathematically based on the feature points obtained by the SIFT algorithm. At last, the multiple objects are reconstructed by leveraging the different movement information.

Guo et al. [32] proposed a motion error compensation method for PSP using Lucas-Kanade optical flow method [56]. The optical flow method makes an initial estimation of the motion by capturing images of the object in the beginning and end state. By using this displacement data and the phase map estimated from a five-step phase shifting method, the displacement of each pixel (d) is computed. Unlike the traditional unwrapping process of adding 2π at discontinuous locations, a compensation (using neighborhood pixels) is performed (using the displacement d) to precisely solve for the phase jump caused by ideal phase shift and the object motion. The main advantage of the method is that, it uses the displacement information obtained from Lucas-Kanade optical flow method to perform motion error compensation and does not depend on any iterative methods for convergence. The limitation is that, the motion information of the object should be estimated beforehand and the method does not work for non-uniform motion.

Duan et al. [33] developed an adaptive reference phase error compensation method to alleviate the errors caused by 2D motion of the object. The errors in the phase map of the moving object is compensated using the phase map of two reference planes (one in front of the object and one behind the object). A traditional PSP method is used for obtaining the phase map of the reference planes. But in this case, markers are used along with the fringe patterns. Markers serve as cues to precisely track the motion of the object. The translation vector (T) and rotation angle (θ) corresponding to the object motion are then estimated. These two parameters (T and θ) are used to unwrap the phase map of the reference planes. As these two planes are not closer to the surface of the object, an adaptive reference phase map is computed using the unwrapped phase maps of the reference planes. Unlike the two reference planes, the adaptive phase map is near to the object in 3D space, so it is directly used for compensating the errors in the phase map of the object. The main advantage of this method is that, there is no need to filter the fringe image to separate the markers from the fringe patterns as they do not overlap. But this method is limited to 2D motion of objects.

In summary, the object tracking methods compensates the phase shift error by tracking the position of the object at various time periods. The methods are effective in reducing the errors induced by uniform motion along any particular axis. However, the methods might not be effective in reducing the phase shift errors when the object undergoes 3D non-uniform motion.

2.3.2. Fourier assisted methods

As we discussed in Section 2.2, the motion-induced error occurs because the object moves within the fringe projection period of PSP. On the other hand, Fourier transform profilometry (FTP) only requires one fringe pattern to retrieve the phase map, thus the object can be regarded as static under only one pattern. One single fringe image can be mathematically described as:

$$I(x,y) = I'(x,y) + I''(x,y)\cos[\phi(x,y)] \tag{7}$$

where $I'(x,y)$ denotes the average intensity, $I''(x,y)$ represents the intensity modulation, and $\phi(x,y)$ is the phase information to be extracted. From Euler's formula, Eq. (7) can be rewritten as:

$$I(x,y) = I'(x,y) + \frac{I''(x,y)}{2}[e^{j\phi(x,y)} + e^{-j\phi(x,y)}] \tag{8}$$

Then, we can preserve only one of the conjugate frequency components as the final image by a band-pass filter. This final image can be denoted as:

$$I_f(x,y) = \frac{I''(x,y)}{2}e^{j\phi(x,y)} \tag{9}$$

With the final image, the phase can be calculated by,

$$\phi(x,y) = \tan^{-1}\left\{\frac{\mathrm{Im}[I_f(x,y)]}{\mathrm{Re}[I_f(x,y)]}\right\} \tag{10}$$

where $\mathrm{Im}[I_f(x,y)]$ and $\mathrm{Re}[I_f(x,y)]$ represent the real part and the imaginary part of the final image $I_f(x,y)$, respectively. Note this phase map, $\phi(x,y)$, is a wrapped phase with 2π discontinuities due to the property of the arctangent function. Additional operations are required to unwrap $\phi(x,y)$. In summary, Eqs. (7) - (10) provide a phase map using only one fringe image, and this phase map is not affected by motion-induced error. A series of methods have incorporated FTP to reduce the motion-induced error, which will be discussed in this section.

Breitbarth et al. [35] first proposed to use FTP algorithm to recover coarse 3D point clouds with each fringe image to estimate the motion. The authors adopted the four-step PSP algorithm, and extracted the phase maps from each fringe image using FTP. Then, they used these phase maps to reconstruct coarse 3D point clouds. To estimate the motion, they utilized the iterative closest points (ICP) algorithm [57]. Given two 3D point clouds, this method essentially finds the best transformation to minimize the distances of the two point clouds. They used ICP to correct the 3D point clouds generated by different fringe images, and then calculated the 2D rear projection of the 3D point clouds through previous system calibration. These coarse 3D point clouds were distinct from the final shape, but they were used for motion estimation. After performing motion compensation by ICP, the 2D rear projections can serve as compensated fringe images in PSP algorithm. Additional gray coded patterns were adopted in this study for phase unwrapping. The authors also explored the qualitative relationship between the relative 3D error and the motion estimation error by performing a simulation. The authors concluded that the accuracy of the motion estimation can be impacted by the poor 3D point clouds (the ones generated by FTP). In addition, the authors investigated the error induced by image blurry. Compared with motion estimation errors, the influence of the blurred images was low. However, one of the limitations of this study is that the authors did not explain how motion would impact the unwrapping process. Gray coding is essentially a temporal phase unwrapping, so the object to be measured may also move in between the gray coded patterns, which can result in significant unwrapping error.

Cong et al. [36] proposed to combine the FTP algorithm with the three-steps PSP algorithm to improve the quality of the phase map. Due to the existence of the motion, the phase shift will no longer be $2\pi/3$, but become two unknowns which are denoted as θ_1 and θ_2. Thus Eqs. (1) - (3) was modified as:

$$I_1(x,y) = I'(x,y) + I''(x,y)\cos[\phi(x,y) - \theta_1], \tag{11}$$

$$I_2(x,y) = I'(x,y) + I''(x,y)\cos[\phi(x,y)], \tag{12}$$

$$I_3(x,y) = I'(x,y) + I''(x,y)\cos[\phi(x,y) + \theta_2]. \tag{13}$$

The phase ϕ can be calculated as:

$$\phi(x,y) = \tan^{-1}\left\{\frac{1-\cos(\theta_2) + [1-\cos(\theta_2)]h}{\sin(\theta_1)h - \sin(\theta_2)}\right\} \tag{14}$$

$$h = \frac{I_2 - I_3}{I_1 - I_2} \tag{15}$$

Each single fringe image, I_1, I_2, and I_3 can all produce phase maps using Eqs. (7) - (10), and they can then be utilized for θ_1 and θ_2 estimation:

$$\Theta_1 = \mathrm{FTP}[I_2] - \mathrm{FTP}[I_1], \tag{16}$$

$$\Theta_2 = \mathrm{FTP}[I_3] - \mathrm{FTP}[I_2] \tag{17}$$

where $\mathrm{FTP}[\cdot]$ denote the phase map extraction operation using the FTP method. The phase map extracted using Eqs. (14) - (17) is more accurate compared to a typical FTP method because the motion-induced error in two adjacent frames can be partially canceled out in the subtraction operation. The quality of the phase map is further improved by a local refinement. Each pixel, (x, y) in the phase map, is corrected by linear fitting using its K-nearest neighbors. Though Cong's method [36] showed significant error reduction for slow, fast and non-uniform motion, there are still some limitations. First, this method is not suitable for non-rigid motion since the local refinement is performed under the rigid motion assumption. Second, spatial phase unwrapping only provides a relative unwrapped phase instead of absolute unwrapped phase. Since the phase value of a spatially unwrapped phase map relies on a starting point of a connected component, spatial unwrapping algorithm cannot accurately reconstruct a 3D scene of various spatially isolated objects.

Li et al. [37] proposed to combine FTP and PSP methods to mitigate the motion-induced error and retrieve an absolute phase map. The authors proposed to use four fringe images in total. These four fringe images include one high-frequency phase-shifted pattern and three low-frequency phase-shifted pattern. First, the high-frequency pattern was utilized to retrieve a wrapped phase map using FTP. Then, a spatial unwrapping algorithm [58] was adopted to calculate the relative unwrapped phase map (Φ_r). For spatially isolated objects in the scene, this relative unwrapped phase map cannot correctly reconstruct their position, as we discussed in the previous paragraph. To determine their absolute phase, the authors first used the three low-frequency phase-shifted patterns with the PSP algorithm to retrieve the wrapped phase, and then followed by a phase unwrapping algorithm using a geometric constraint approach [59], which eventually results in an absolute unwrapped phase map (Φ_e). This was used for determining the fringe order of the FTP calculated relative phase map. They computed the difference map k_e in fringe order between Φ_r and Φ_e:

$$k_e = \text{round}\left\{ \left[\Phi_e(u + \Delta u, v + \Delta v) \times \frac{T^l}{T} - \Phi_r(u, v) \right] / (2\pi) \right\} \tag{18}$$

In Eq. (18) Δu and Δv are introduced to compensate the motion, which are determined by detecting the motion of the central pixel of the bounding box for each isolated object in the adjacent fringe images. The fringe periods of the low frequency pattern and the high frequency pattern are denoted as T^l and T, respectively. Then, the rigid shift k_s in fringe order between the relative phase map and the absolute phase map can be obtained as the most common integer on the k_e map:

$$k_s = \text{mode}[k_e(u, v)] \tag{19}$$

Finally, the absolute phase map can be retrieved:

$$\Phi_a(u, v) = \Phi_r(u, v) + 2\pi \times k_s \tag{20}$$

The advantage of this method is that it is capable of scanning scenes with multiple isolated objects. However, the method essentially uses FTP to retrieve the phase map, which has inherent limitations of the FTP approach. For example, FTP method cannot accurately retrieve the phase map when local surfaces have large geometrical or texture variations. Moreover, since the method uses spatial unwrapping, its performance can be affected when abrupt geometric discontinuities occur in the scene.

Qian et al. [38] proposed to use the FTP method and the PSP method respectively on the dynamic regions and the static regions in the scene. The authors used four fringe patterns (one pure white pattern and three phase-shifted fringe patterns). For the FTP process, the second fringe image in the phase-shifting fringes was selected to extract the phase map. The authors demonstrated that the most cases of motions are translational and rotation motion, where the PSP result fluctuates around the FTP result of the second fringe pattern. The wrapped phase map retrieved by FTP was unwrapped by the stereo phase unwrapping (SPU) method [60]. For the PSP process, the extracted phase map was also unwrapped by this SPU method. The next step is to combine the two phase maps from PSP and FTP. The final phase map is obtained by replacing the region affected by motion in PSP phase map with the corresponding region in FTP phase map. To distinguish them, the authors proposed the phase frame different method (PFDM). First, the pixel-wise differences of the phase maps from two adjacent frames retrieved by FTP was calculated. Then, this differences map was binarized according to certain threshold: if the value of a pixel is large than the threshold, then it becomes 1, otherwise 0. The threshold was setup to compensate the phase difference resultinged from imaging noise, which was determined by continuously scanning one static plane, and studying the phase variations. This binarized map essentially serves as region detector. Namely, in this binarized map, the regions with value of 1 represent dynamic region, and the regions with value of 0 represent static region. Finally, the phase map from PSP and the phase map from FTP were fused together according to the binarized map, where regions of 1 use the FTP phase map, and regions of 0 use the PSP phase map. Qian's method [38] solves the motion-effected region using FTP effectively and maintain the high quality of the phase map using PSP. As the method unwraps the phase by SPU, it avoids using auxiliary fringe patterns (e.g., the low frequency patterns in temporal phase unwrapping), thereby the speed of the measuring process is increased. However, the price is that it requires an additional camera, which increases the cost and the complexity of the system. Another limitation is that, the dynamic region still has the inherent limitation of the FTP approach. The measurement accuracy can be limited when high depth variation occurs.

Guo et al. [39] developed a Fourier transform based motion-induced error reduction method using dual-frequency composite phase-shifted grating patterns. The method involved projecting dual frequency composite grating fringes on to the object. Two sets of phase maps (PSP and FTP) were calculated from the camera captured fringe images. First, the FTP based phase map is calculated from the latest fringe image. Then, the phase map obtained using PSP is used for initial 3D reconstruction. In order to locate the regions in the phase map (PSP based) that are affected by motion, a virtual high frequency phase map is used. The virtual high frequency phase is viewed as the phase map of the object in the static condition. The region affected by motion in the phase difference map (between virtual and high frequency phase map) is obtained by performing a threshold binarization. Similarly, the modulation ratio between the static (virtual high frequency phase map) and the dynamic phase map (PSP based phase map) was also estimated. The motion region was obtained by the intersection of the phase difference and modulation ratio. The region identified to have motion errors (in PSP phase map) is replaced with the corresponding region in FTP phase map. The advantage of this method is that it can perform an accurate 3D reconstruction of complex scenes with dynamic and static objects. However, the method might not be used in case of dynamically deformable objects, as it does a region-wise error compensation instead of a pixelwise error compensation.

In summary, FTP-assisted motion-induced error compensation methods are effective in resolving the errors induced by high-speed motion given that FTP extracts phase with only a single-shot fringe image. However, these FTP-based approaches are subject to the inherent limitations of FTP including the impaired phase quality caused by noises or textural variations.

2.3.3. Motion prediction

The phase shifting errors caused by moving object can be reduced if the motion can be predicted. This section will discuss the different solutions that reduces the phase shift error by predicting the object's motion. Weise et al. [41] developed a GPU assisted motion reduction method for a binocular vision system. The authors developed a numerical model to compensate for the phase errors caused by object's motion. Using the interframe delay (between two successive camera captures), the velocity of the surface points was estimated. With the velocity, the shift in object's position was estimated for every pixel and the phase map was corrected accordingly. The main advantage of the method is that it can perform a pixel level motion error compensation. However, the method cannot handle non-uniform motion.

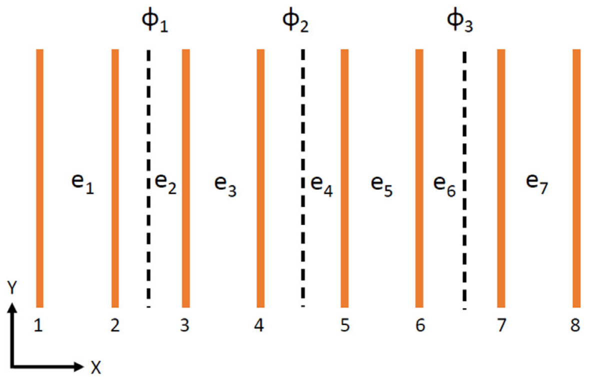

Fig. 2. Eight successive frames of a moving object with the phase shift error.

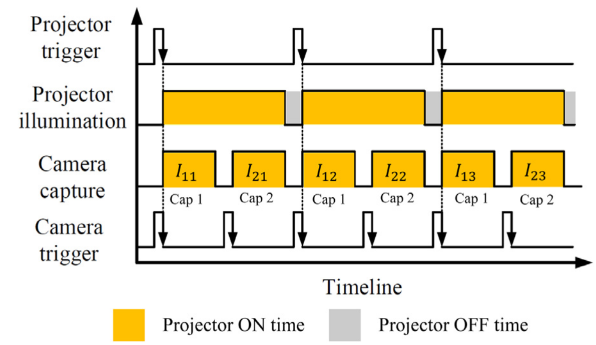

Fig. 3. Timing chart for additional temporal sampling.

Han et al. [42] proposed another method for compensating the motion-induced errors in a binocular vision system. The method is applicable to multi-frequency PSP system. From the first frequency, the pixel movement is estimated by identifying the corresponding pairs in the phase-shifted fringe images. The features in the object serve as cues for identifying the corresponding pairs. The corresponding pairs of all the pixels is stored in the form of a homography matrix. This homography matrix is used for compensating the phase error in the fringe patterns corresponding to the second frequency. The main advantage of this method is that it is automated and does a pixelwise motion error compensation. However, the method might not work for objects with a uniform texture as it will be difficult to estimate the homography matrix.

Liu et al. [43] compensated the motion-induced errors by estimating the phase shift in the projector's imaging plane. The authors established a relationship between the object's motion (Δx, Δy and Δz) and projector's imaging plane coordinates (u and v). The motion of the object is estimated by comparing the 3D coordinates of the same point in different frames and this information is used to compensate for the phase shift errors. The motion is estimated by subtracting two 3D geometries obtained from two sets of phase shifted fringe patterns. Using the pinhole model of the projector, a relationship is established between the phase and the object motion. By using this relationship and the motion estimated from the two 3D geometries, the phase shift error for each pixel can be obtained. In this way, the phase shift error for each pixel is estimated. An iterative approach is used to obtain an enhanced 3D geometry. The method is effective in reducing the motion errors for dynamically deformable objects as it does a pixelwise error compensation. However, an assumption underlying this approach is that the camera capturing speed is high enough to ignore the pixel disparities of the objects in successive frames, which may be violated if the objects move at high speeds.

Liu et al. [44] proposed a method of compensating the motion errors in a phase map using three phase maps. The authors established a motion error compensation method for 4-step phase shifted fringe patterns. Eight consecutive images of four step fringe patterns are captured for a moving object (as shown in Fig. 2). Three phase maps (ϕ_1, ϕ_2 and ϕ_3) are estimated from the eight images treating them as three sets of four-step phase shifted fringe patterns. The phase error ($\Delta\phi$) of each phase map (ϕ) was expressed in terms of the phase shift errors (e) (in that corresponding time period) and upon Taylor expansion it was approximated to the expression described in Eq. 21.

$$\Delta\phi_1 = \frac{e_3 - e_1}{4} + \frac{e_3 + e_1}{4} cos 2\phi_1. \tag{21}$$

By performing an averaging operation, the phase shift errors was computed from the phase maps obtained from the three sets of fringe patterns. The phase maps are expressed in terms of the phase shift errors (e). The error compensated phase map is obtained by updating the phase of the fringe patterns. The experimental results indicates that the error compensation method works well for surfaces with large depth variations. However, the method is limited to objects that undergo uniform translation motion.

Wang et al. [45] developed a novel motion-induced error compensation method using additional temporal sampling. Unlike conventional PSP, the system uses defocused binary patterns. The method takes advantage of the binary defocusing method to separate the motion-induced phase error (from the fixed phase shift) by performing additional temporal sampling. As binary defocusing method does not require a rigid camera projector synchronization, two images were captured in one projector cycle (additional temporal sampling). The timing chart for additional temporal sampling is shown in Fig. 3. Two sets of three-step phase shifted (Cap 1 and Cap 2 in Fig. 3) patterns are obtained. The motion-induced phase error can be estimated by computing the difference between the phase maps of the two set of fringe patterns $I_{11} - I_{31}$ and $I_{12} - I_{32}$ (as shown in Eq. (22) - (27)).

$$I_{11}(x, y) = I'(x, y) + I''(x, y)\cos[\Phi(x, y) - 2\pi/3], \tag{22}$$

$$I_{21}(x, y) = I'(x, y) + I''(x, y)\cos[\Phi(x, y) + \delta], \tag{23}$$

$$I_{31}(x, y) = I'(x, y) + I''(x, y)\cos[\Phi(x, y) + 2\pi/3 + 2\delta], \tag{24}$$

$$I_{12}(x, y) = I'(x, y) + I''(x, y)\cos[\Phi(x, y) - 2\pi/3 + \delta/2], \tag{25}$$

$$I_{22}(x, y) = I'(x, y) + I''(x, y)\cos[\Phi(x, y) + \delta + \delta/2], \tag{26}$$

$$I_{32}(x, y) = I'(x, y) + I''(x, y)\cos[\Phi(x, y) + 2\pi/3 + 2\delta + \delta/2]. \tag{27}$$

Then, an iterative operation is performed to compensate the phase error of the two phase maps. The main advantage of the method is that it does motion error compensation without compromising on measurement speed (i.e., the motion error is compensated with the images captured in one projector cycle). Moreover, as binary patterns are used, the method is applicable for high-speed applications. However, given that the method relies on the accuracy of the external trigger (for capturing two images in one cycle), there might be residual errors in the final geometry if there is delay in the trigger.

In summary, the motion prediction methods are effective in reducing the phase shift errors for dynamically deforming objects as there is a pixelwise error compensation. However, these methods might not be perform an effective error compensation in few scenarios: (i) object undergoes non-uniform motion [41,44] and (ii) when the motion information cannot be precisely obtained beforehand [43].

2.3.4. Other methods

Feng et al. [46] classified the motion-induced errors into three categories: (i) motion ripples, (ii) phase unwrapping errors and (iii) motion outliers. The motion ripples here refer to the additional phase shift caused by the object motion. The object is segmented into small patches and the error compensation is performed on these segmented regions.

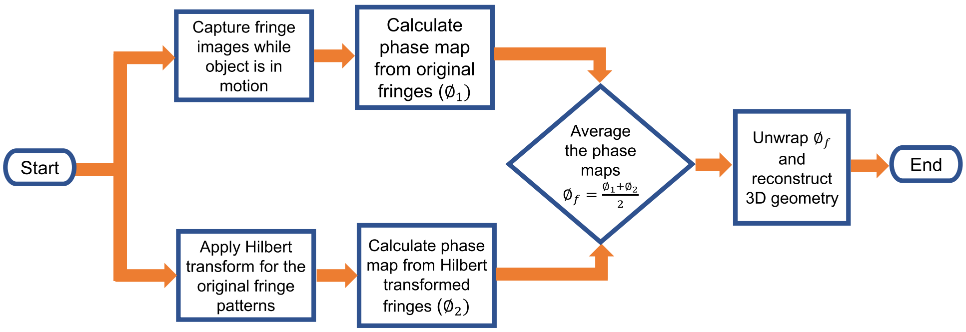

Fig. 4. Schematic of the motion error reduction method using Hilbert transform.

An initial guess of the motion is made by adding an error term in the phase shifted fringe images. The average phase shift obtained by comparing the segmented patches is used to solve the phase error in the phase map. An iterative operation is performed to reduce the errors in the phase map. In the case of phase unwrapping errors, if the phase value of a pixel is more than a threshold, then it is corrected by using the neighborhood pixel information. The motion outliers are identified by comparing the phase map with the corresponding blurred result and are removed if the difference is more than a certain threshold. The advantage of the method is that it does not require additional set of fringe patterns for motion error compensation, thereby it does not compromise on the measurement speed. However, the method is not applicable for dynamically deforming objects and rotational motion, as it does not perform a pixelwise error compensation.

Wang et al. [47] developed a novel motion error reduction method using Hilbert transform. The authors proved that the phase error introduced by motion approximately doubles the frequency of the fringe pattern. It was also found that, the phase map obtained by performing Hilbert transform to the phase shifted fringe patterns had a distribution opposite to that of the original phase map. Therefore, the phase map of the regular phase shifted patterns and Hilbert transformed patterns are averaged to cancel out the errors introduced by motion. The schematic of the method is illustrated in Fig. 4. The advantage of the method is that it can reduce the motion-induced errors for rigid moving objects and dynamically deforming objects. However, the method will require additional processing for compensating the errors at the fringe edges.

Yu et al. [48] employed the deep learning to reconstruct the moving object. The algorithm only requires one or two fringe patterns, leading to reducing the errors caused by motion. An end-to-end deep convolution neural network is utilized to transform the single or two fringe patterns into multiple phase shifted sinusoidal fringe patterns. At last, the phase information is calculated by the generated fringe patterns. The method reconstructs the moving object by reducing the fringe number, which did not address the issues in PSP directly.

3. Comparative evaluation

3.1. Test system

We built a test system to provide a comparative evaluation of the various motion-induced error reduction methods for phase shifting profilometry. The system setup consists of a DLP developmental kit (model: Texas Instrument DLP LightCrafter 4500) for fringe pattern projection and a complimentary-metal-oxide-semiconductor (CMOS) camera (model: FLIR Grasshopper3 GS3-U3-23S6C-CGS3-U3-41C6C-C) for image acquisition. The camera is attached to a 8 *mm* focal length lens. The camera resolution was set to 514 × 544 pixels, and the projector was set to the native resolution of 912 × 1140 pixels. In our research, we used three square binary patterns with a fringe period of 18 pixels for phase retrieval and another set of binary dithered patterns with a fringe period of 240 pixels for phase unwrapping. We used the enhanced two-frequency phase-shifting method proposed by Hyun and Zhang [61] for absolute phase retrieval. An artificial ideal phase map is generated at the minimum depth plane of the measurement volume, which is leveraged to unwrap the low-frequency phase. The camera capture rate was set to 166 Hz, and the projector was configured to project fringe patterns at 83 Hz. A programmable microcontroller (Arduino UNO) was used to precisely control the projector and camera. In the following comparative evaluations, we selected one method from each of the four categories as discussed in Section 2, including an object tracking-based approach [26], a Fourier-assisted approach [37], a motion prediction-based approach [45], and an other method (based on Hilbert transform) [47].

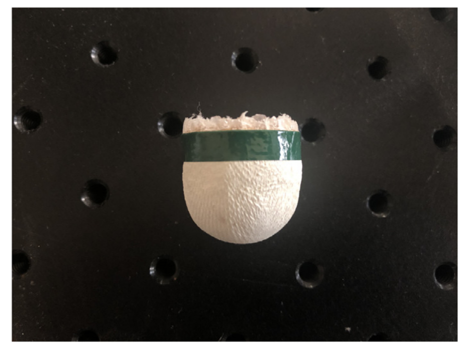

Fig. 5. Snapshot of the badminton birdie.

3.2. Dynamic 3D shape measurement of an object with 2D motion

We first measured a dynamically moving (in-plane 2D motion) badminton birdie (as shown in Fig. 5) for comparative evaluation. The results obtained from the standard phase shifting algorithm as well as the four selected methods [26,37,45,47] are shown in Fig. 6. From the Fig. 6, we can observe that the 3D topography reconstructed by the object tracking method of Lu et al. [26] (as shown in Fig. 6(b)) has the best overall performance. This is because the marker/feature tracking provides cues that can precisely extract the in-plane motion of the birdie during one cycle of fringe projection. The result of Fourier-assisted method (see Fig. 6(c)) has alleviated the motion-induced error in phase shifting due to its single-shot nature in wrapped phase retrieval. However, it is also apparent that this method suffers from the inevitable limitations of Fourier transform with the surface topography being smoothened. The results in Fig. 6(d) - 6(e) show that the motion prediction-based approach [45] and the Hilbert transform-based approach [47] can address the limitation of Fourier transform by preserving the fine details on the surface topography. Within the two approaches, the Hilbert transform-based approach has slightly better performance than the motion prediction-based approach given that it has less restrictions on the assumption of uniform motion within a cycle of pattern projection. However, their overall performance is worse than

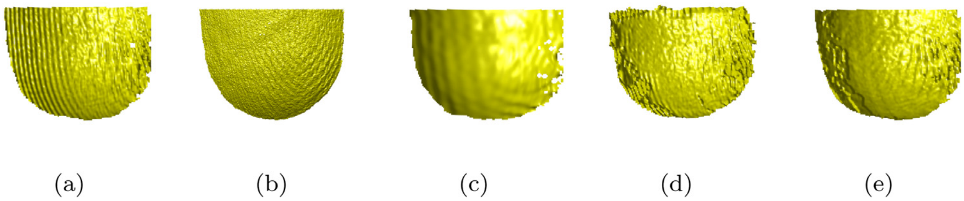

Fig. 6. Experimental results of measuring a dynamically moving (in-plane) birdie. A sample 3D frame reconstructed by (a) the standard phase-shifting algorithm; (b) object tracking method [26]; (c) Fourier assisted method [37]; (d) motion prediction method [45] and (e) other method (Hilbert transform [47]).

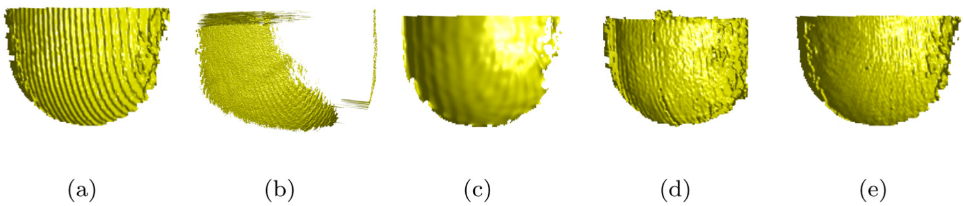

Fig. 7. Experimental results of measuring a dynamically moving (out-of-plane) birdie. A sample 3D frame reconstructed by (a) the standard phase-shifting algorithm; (b) object tracking method [26]; (c) Fourier assisted method [37]; (d) motion prediction method [45] and (e) other method (Hilbert transform [47]).

the marker-based approach given that they cannot extract 2D motion as precise as marker/feature tracking. In addition, both methods have problems in reconstructing the boundaries accurately.

3.3. Dynamic 3D shape measurement of an object with 3D motion

To provide a thorough evaluation, we also conducted an additional experiment by measuring the same object with out-of-plane 3D motion. The results obtained from the standard phase shifting algorithm as well as the four selected methods [26,37,45,47] are shown in Fig. 7. Fig. 7(b) shows the result obtained from the marker tracking-based method 7(b), from which one can clearly see that this method would fail in the scenario of 3D motion given that the nature of marker/feature tracking is constrained 2D image. For the other three methods, the observation is the same as the previous case with 2D motion. Specifically, the Fourier-assisted method [37] can alleviate the motion-induced error due to its single-shot nature in wrapped phase retrieval, yet the fine-scale surface details are not well-preserved due to the filtering in the frequency domain (as shown in Fig. 7(c)). Compared to Fourier-assisted approach, the motion prediction-based method [45] and Hilbert transform-based method [47] can maintain the details in the reconstructed 3D surface geometry. The latter has better overall performance than the former due to the fact that the former method assumes that the object moves uniformly within a cycle of pattern projection. In the meantime, both methods still suffer slightly from the edge problem in 3D reconstruction.

4. Discussion

4.1. Method selection

In Section 2, the algorithms reducing the errors caused by the object motion have been reviewed. Different movement introduces different types of errors. As existing methods have diverse advantages and limitations, there is no single algorithm that can be immune to the errors caused by different movement. The selection of the correct method for a specific application hinges on the identification of a number of properties, including the required number of patterns, rigid object or free transform object, uniform motion or free motion, 2D movement or 3D movement, single smooth object or multiple isolated objects, etc. We summarized some classical algorithms with comparative analysis of these properties as shown in Fig. 8. Following are some of the observations:

(1) *The influence of the number of fringe patterns used*. As this paper only discusses the methods based on PSP, most existing algorithms need at least three fringe patterns to reconstruct the object. For the moving object reconstruction with traditional PSP, the reconstruction accuracy will be decreased when the fringe pattern number is increased. On the other hand, the object tracking based methods utilize the movement information among the different fringe patterns directly, which can remove the influence caused by the movement. The Fourier-assisted methods and the motion prediction methods are more sensitive to the number of fringe patterns used.

(2) *The ability to accurately reconstruct non-rigid objects*. Most methods are limited to the reconstruction of the rigid object. All the methods based on object tracking only can reconstruct the rigid object. Given that it is hard to obtain a mathematical description for the movement of non-rigid object, using object-tracking only can be challenging in performing an effective analysis on the physics and thus difficult to perform an accurate 3D reconstruction. The advantage of FTP is that it can extract phases with a single fringe pattern, and thus an accurate 3D reconstruction of non-rigid objects can be made possible. For instance, Ref. [38] as an example of FTP-assisted approach employs hybrid FTP and PSP method to reconstruct the scene consisting of both static and dynamic objects. The FTP is utilized to reconstruct the dynamic part and PSP is used to reconstruct the static/quasi-static part. The motion prediction methods can also partially address the 3D reconstruction of non-rigid object due to its ability to predict motion on a pixel-by-pixel basis. For instance, Ref. [43] is an example of the motion prediction method which can predict the movement pixel-by-pixel, leading to good performance when the deformed object is reconstructed.

(3) *The ability to resolve non-uniform motion*. The uniform motion means that the object movement is limited in the speed and direction of motion (such as constant speed or one direction movement). Most methods require that the object exhibits uniform motion. Compared with the non-uniform motion, the influence caused by the uniform motion is simple and homogeneous, leading to convenience on the prediction of the motion. For example, most motion prediction methods such as Ref. [42–44], the object movement is assumed to remain constant between the fringe patterns. On the other hand, for the object tracking-based methods in Ref. [26–29], as the object movement among the fringe patterns is tracked and described mathematically, there is no such limitation on the direction and speed of the movement.

(4) *The ability to resolve different types of motion*. The ability to perform 3D reconstruction under different types of movements is another key property in algorithm selection. 3D movement is the free movement in $x - y - z$ dimension and non-3D movement is the translational and/or rotational movement without variation along the z-direction. Given that the 3D movement introduces the variations along depth and such information typically remains to be solved, it is hard to obtain the mathematical description for 3D movement, which results in the fact that the object tracking-based methods cannot reconstruct the objects with 3D movement. In contrast, taking the advantages of the single fringe pattern reconstruction, the Fourier-assisted methods have the ability to reconstruct the object with 3D movement. In addition, most of the mo-

Algorithm category	Reference number	Pattern number	Rigid object	3D movement	Uniform motion	Isolated objects	Individual movement	Computational efficient
Object tracking	Ref. 26, 28	⩾3	Y	N	N	N	N	Y
	Ref. 27, 29	⩾3	Y	Y	N	N	N	Y
	Ref. 30	⩾3	Y	N	Y	N	N	Y
	Ref. 31	⩾3	Y	N	N	Y	N	Y
	Ref. 34	⩾3	Y	N	N	Y	Y	Y
	Ref. 32	⩾5	Y	Y	Y	N	N	Y
	Ref. 33	⩾3	Y	N	N	N	N	Y
Fourier assisted methods	Ref. 35	4	Y	Y	N	Y	N	N
	Ref. 36	3	Y	Y	N	N	N	N
	Ref. 37	4	Y	Y	N	Y	N	N
	Ref. 38	4	Y	Y	N	Y	N	N
	Ref. 39	≥3	Y	Y	N	Y	N	N
Motion prediction	Ref. 41	⩾3	Y	Y	N	Y	N	N
	Ref. 42	⩾6	Y	N	Y	Y	N	Y
	Ref. 43	⩾3	N	Y	N	N	N	N
	Ref. 44	4	Y	Y	Y	N	N	Y
	Ref. 45	⩾6	Y	Y	Y	N	N	Y
Other methods	Ref. 46	⩾3	Y	N	Y	N	N	N
	Ref. 47	⩾3	Y	Y	N	N	N	Y

Fig. 8. Comparison of different algorithms.

tion prediction methods can reconstruct the object with 3D movement by assuming the movement to be uniform.

(5) *The ability to resolve isolated objects*. When isolated objects are present, temporal phase unwrapping methods with additional fringe patterns are typically required to unwrap the phase. The movement between the additional fringe patterns will aggravate the reconstruction errors. The situation is more severe for the object tracking methods employing the movement information among all the fringe patterns. Only Ref. [31] can reconstruct the isolated objects by analyzing the influence of movement between the additional fringe patterns for phase unwrapping and the fringe patterns for phase retrieval. For the Fourier-assisted methods and motion prediction methods, Ref. [37,38,41,42] reconstruct the isolated objects by employing the stereo phase unwrapping or multi-frequency unwrapping method.

4.2. Future work

We identify the following directions as potential opportunities for future research work.

(1) *Tracking based algorithms allowing free 3D movement*. As the information of dynamic motion is directly extracted, the tracking based algorithms may have the potential to fundamentally address the errors caused by the movement. However, to our best knowledge, the tracking based algorithms cannot reconstruct the object with free 3D movement and the object movement is limited to 2D. This is due to the fact that it is difficult to extract 3D movement information as the movement along depth direction is hard to estimate in nature. Therefore, a tracking algorithm capable of compensating the motion in 3D is needed in state-of-the-art.

(2) *Application of technologies into diversified scene to address the specific issues caused by movement*. Although there are many existing works focusing on dynamic object reconstruction, there is no one single method to address all the issues in real application scenario. Taking the case of assembly line as an example, the object does not undergo pure 2D motion, since motion along the depth direction is also introduced by vibration when it is transferred from one point to another. Therefore, a method that can address diversified scenes is needed for real-world practices.

(3) *Robust 3D reconstruction of deforming objects*. Most of the existing approaches address the problem of rigid body motion, but the reconstruction of deforming objects is also of significant importance and spans a wide range of applications. Some of the applications include tensile testing of materials and fluid deposition process. Exploring advanced algorithms that can address object deformations will further expand the boundary of PSP algorithms.

5. Summary

This paper summarized the existing works regarding the reduction of motion-induced measurement errors in PSP. Advances have been made to address the 3D shape measurement errors using approaches based on different principles including (i) object tracking, (ii) Fourier assisted methods, (iii) motion prediction and (iv) other methods. The experimental results demonstrate the effectiveness of the algorithms in compensating the motion-induced errors in measuring a dynamic object. The capabilities and boundaries of these technologies are discussed to provide guidance for researchers to select the proper method according to the specific application. Future efforts will be focused on developing methods to robustify the motion-induced error reduction with diversified application scenarios.

Declaration of Competing Interest

The authors declare that they have no known competing financial interests or personal relationships that could have appeared to influence the work reported in this paper.

CRediT authorship contribution statement

Lei Lu: Investigation, Methodology, Software, Supervision, Writing - original draft. **Vignesh Suresh:** Investigation, Methodology, Software, Visualization, Writing - original draft. **Yi Zheng:** Software, Writing - original draft. **Yajun Wang:** Investigation, Methodology, Writing - review & editing, Supervision. **Jiangtao Xi:** Investigation, Methodology, Supervision. **Beiwen Li:** Investigation, Resources, Writing - review & editing, Supervision, Project administration, Funding acquisition.

Acknowledgments

This work is funded by Iowa State University (College of Engineering Faculty Startup fund) and Natural Science Foundation of China (NSFC) (61705060, 61603360).

References

[1] Gorthi SS, Rastogi P. Fringe projection techniques: whither we are? Opt Lasers Eng 2010;48(ARTICLE):133–40.
[2] Pettersson B.. Coordinate measuring machine. 2009. US Patent 7,591,077.
[3] Bieg L.F., Jokiel Jr B., Ensz M.T., Watson R.D.. Highly accurate articulated coordinate measuring machine. 2003. US Patent 6,668,466.
[4] Bailey R.-P. S.. Coordinate measuring machine. 2010. US Patent 7,793,425.
[5] Park J-j, Kwon K, Cho N. Development of a coordinate measuring machine (cmm) touch probe using a multi-axis force sensor. Meas Sci Technol 2006;17(9):2380.
[6] Meli F, Küng A. Afm investigation on surface damage caused by mechanical probing with small ruby spheres. Meas Sci Technol 2007;18(2):496.
[7] Dorsch RG, Häusler G, Herrmann JM. Laser triangulation: fundamental uncertainty in distance measurement. Appl Opt 1994;33(7):1306–14.
[8] Kolb A, Barth E, Koch R, Larsen R. Time-of-flight cameras in computer graphics. In: Computer Graphics Forum, 29. Wiley Online Library; 2010. p. 141–59.
[9] Chiabrando F, Chiabrando R, Piatti D, Rinaudo F. Sensors for 3d imaging: metric evaluation and calibration of a ccd/cmos time-of-flight camera. Sensors 2009;9(12):10080–96.
[10] Subbarao M, Surya G. Depth from defocus: a spatial domain approach. Int J Comput Vis 1994;13(3):271–94.
[11] Chaudhuri S, Rajagopalan AN. Depth from defocus: a real aperture imaging approach. Springer Science & Business Media; 2012.
[12] Marr D, Poggio T. A computational theory of human stereo vision. Proceedings of the Royal Society of London Series B Biological Sciences 1979;204(1156):301–28.
[13] Yamashita A, Kawarago A, Kaneko T, Miura KT. Shape reconstruction and image restoration for non-flat surfaces of documents with a stereo vision system. In: Proceedings of the 17th International Conference on Pattern Recognition, 2004. ICPR 2004., 1. IEEE; 2004. p. 482–5.
[14] Zhang S. Recent progresses on real-time 3d shape measurement using digital fringe projection techniques. Opt Lasers Eng 2010;48(2):149–58.
[15] Zhang S, Van Der Weide D, Oliver J. Superfast phase-shifting method for 3-d shape measurement. Opt Express 2010;18(9):9684–9.
[16] Zhang S. High-Speed 3D imaging with digital fringe projection techniques. CRC Press; 2018.
[17] Takeda M, Mutoh K. Fourier transform profilometry for the automatic measurement of 3-d object shapes. Appl Opt 1983;22:3977–82.
[18] Malacara D. Optical shop testing, 59. John Wiley & Sons; 2007.
[19] Zhang S. High-speed 3d shape measurement with structured light methods: a review. Opt Lasers Eng 2018;106:119–31.
[20] Zhang S. Absolute phase retrieval methods for digital fringe projection profilometry: a review. Opt Lasers Eng 2018;107:28–37.
[21] Cui H, Liao W, Dai N, Cheng X. A flexible phase-shifting method with absolute phase marker retrieval. Measurement 2012;45(1):101–8.
[22] Huang L, Asundi AK. Practical framework for phase retrieval and invalidity identification with temporal phase unwrapping method in fringe projection profilometry. In: Applied Mechanics and Materials, 83. Trans Tech Publ; 2011. p. 179–84.
[23] Zhang S, Huang PS. Novel method for structured light system calibration. Opt Eng 2006;45(8):083601.
[24] Lei S, Zhang S. Flexible 3-d shape measurement using projector defocusing. Opt Lett 2009;34(20):3080–2.
[25] Gong Y, Zhang S. Ultrafast 3-d shape measurement with an off-the-shelf dlp projector. Opt Express 2010;18(19):19743–54.
[26] Lu L, Xi J, Yu Y, Guo Q. New approach to improve the accuracy of 3-d shape measurement of moving object using phase shifting profilometry. Opt Express 2013;21(25):30610–22.
[27] Lu L, Xi J, Yu Y, Guo Q. Improving the accuracy performance of phase-shifting profilometry for the measurement of objects in motion. Opt Lett 2014;39(23):6715–18.
[28] Lu L, Ding Y, Luan Y, Yin Y, Liu Q, Xi J. Automated approach for the surface profile measurement of moving objects based on psp. Opt Express 2017;25(25):32120–31.
[29] Lu L, Yin Y, Su Z, Ren X, Luan Y, Xi J. General model for phase shifting profilometry with an object in motion. Appl Opt 2018;57(36):10364–9.
[30] Flores JL, Stronik M, Muñoz A, Garcia-Torales G, Ordoñes S, Cruz A. Dynamic 3d shape measurement by iterative phase shifting algorithms and colored fringe patterns. Opt Express 2018;26(10):12403–14.
[31] Lu L, Jia Z, Luan Y, Xi J. Reconstruction of isolated moving objects with high 3d frame rate based on phase shifting profilometry. Opt Commun 2019;438:61–6.
[32] Guo Y, Da F, Yu Y. High-quality defocusing phase-shifting profilometry on dynamic objects. Opt Eng 2018;57(10):105105.
[33] Duan M, Jin Y, Xu C, Xu X, Zhu C, Chen E. Phase-shifting profilometry for the robust 3-d shape measurement of moving objects. Opt Express 2019;27(16):22100–15.
[34] Lu L, Jia Z, Pan W, Zhang Q, Zhang M, Xi J. Automated reconstruction of multiple objects with individual movement based on psp. Opt Express 2020;28(19):28600–11.
[35] Breitbarth A, Kühmstedt P, Notni G, Denzler J. Motion compensation for three-dimensional measurements of macroscopic objects using fringe projection. In: DGaO Proceedings, 113; 2012. p. A11.
[36] Cong P, Zhang Y, Xiong Z, Zhao S, Wu F. Accurate 3d reconstruction of dynamic scenes with fourier transform assisted phase shifting. In: 2013 Visual Communications and Image Processing (VCIP). IEEE; 2013. p. 1–6.
[37] Li B, Liu Z, Zhang S. Motion-induced error reduction by combining fourier transform profilometry with phase-shifting profilometry. Opt Express 2016;24(20):23289–303.
[38] Qian J, Tao T, Feng S, Chen Q, Zuo C. Motion-artifact-free dynamic 3d shape measurement with hybrid fourier-transform phase-shifting profilometry. Opt Express 2019;27(3):2713–31.
[39] Guo W, Wu Z, Li Y, Liu Y, Zhang Q. Real-time 3d shape measurement with dual-frequency composite grating and motion-induced error reduction. Opt Express 2020;28(18):26882–97. doi:10.1364/OE.403474.
[40] Su X, Zhang Q. Dynamic 3-d shape measurement method: a review. Opt Lasers Eng 2010;48(2):191–204.
[41] Weise T, Leibe B, Van Gool L. Fast 3d scanning with automatic motion compensation. In: 2007 IEEE Conference on Computer Vision and Pattern Recognition. IEEE; 2007. p. 1–8.
[42] Han L, Li Z, Zhong K, Cheng X, Luo H, Liu G, et al. Vibration detection and motion compensation for multi-frequency phase-shifting-based 3d sensors. Sensors 2019;19(6):1368.
[43] Liu Z, Zibley PC, Zhang S. Motion-induced error compensation for phase shifting profilometry. Opt Express 2018;26(10):12632–7.
[44] Liu X, Tao T, Wan Y, Kofman J. Real-time motion-induced-error compensation in 3d surface-shape measurement. Opt Express 2019;27(18):25265–79.
[45] Wang Y, Suresh V, Li B. Motion-induced error reduction for binary defocusing profilometry via additional temporal sampling. Opt Express 2019;27(17):23948–58.
[46] Feng S, Zuo C, Tao T, Hu Y, Zhang M, Chen Q, et al. Robust dynamic 3-d measurements with motion-compensated phase-shifting profilometry. Opt Lasers Eng 2018;103:127–38.
[47] Wang Y, Liu Z, Jiang C, Zhang S. Motion induced phase error reduction using a hilbert transform. Opt Express 2018;26(26):34224–35.
[48] Yu H, Chen X, Zhang Z, Zuo C, Zhang Y, Zheng D, et al. Dynamic 3-d measurement based on fringe-to-fringe transformation using deep learning. Opt Express 2020;28(7):9405–18.
[49] Marrugo AG, Gao F, Zhang S. State-of-the-art active optical techniques for three-dimensional surface metrology: a review. JOSA A 2020;37(9):B60–77.
[50] Zuo C, Feng S, Huang L, Tao T, Yin W, Chen Q. Phase shifting algorithms for fringe projection profilometry: a review. Opt Lasers Eng 2018;109:23–59.
[51] Zhang S. High-speed 3d shape measurement with structured light methods: a review. Opt Lasers Eng 2018;106:119–31.
[52] Zhang S. Absolute phase retrieval methods for digital fringe projection profilometry: a review. Opt Lasers Eng 2018;107:28–37.
[53] Zuo C, Huang L, Zhang M, Chen Q, Asundi A. Temporal phase unwrapping algorithms for fringe projection profilometry: a comparative review. Opt Lasers Eng 2016;85:84–103.
[54] Wang Z, Han B. Advanced iterative algorithm for phase extraction of randomly phase-shifted interferograms. Opt Lett 2004;29(14):1671–3.
[55] Zhang S. High-Speed 3D imaging with digital fringe projection techniques. CRC Press; 2016.
[56] Kanade T, Okutomi M. A stereo matching algorithm with an adaptive window: theory and experiment. IEEE Trans Patt Analy and Mach Intellig 1994;16(9):920–32.
[57] Rusinkiewicz S, Levoy M. Efficient variants of the icp algorithm. In: Proceedings Third International Conference on 3-D Digital Imaging and Modeling. IEEE; 2001. p. 145–52.
[58] Zhang S, Li X, Yau S-T. Multilevel quality-guided phase unwrapping algorithm for real-time three-dimensional shape reconstruction. Appl Opt 2007;46(1):50–7.
[59] An Y, Hyun J-S, Zhang S. Pixel-wise absolute phase unwrapping using geometric constraints of structured light system. Opt Express 2016;24(16):18445–59.
[60] Liu X, Kofman J. High-frequency background modulation fringe patterns based on a fringe-wavelength geometry-constraint model for 3d surface-shape measurement. Opt Express 2017;25(14):16618–28.
[61] Hyun J-S, Zhang S. Enhanced two-frequency phase-shifting method. Appl Opt 2016;55(16):4395–401.